



Semnan University

Mechanics of Advanced Composite Structures

journal homepage: <http://macs.journals.semnan.ac.ir>

Nonlocal Buckling and Vibration Analysis of Triple-Walled ZnO Piezoelectric Timoshenko Nano-beam Subjected to Magneto-Electro-Thermo-Mechanical Loadings

M. Mohammadimehr*, S.A.M. Managheb, S. Alimirzaei

Department of Solid Mechanics, Faculty of Mechanical Engineering, University of Kashan, Kashan, Iran

PAPER INFO

Paper history:

Received 30 October 2015

Received in revised form 7 January 2016

Accepted 31 January 2016

Keywords:

Non-local buckling and vibration analysis

Triple-walled ZnO piezoelectric Timoshenko nano-beam

Elastic foundation

Magneto-electro-thermo-mechanical loadings.

ABSTRACT

In this study, using the non-local elasticity theory, the buckling and vibration analysis of triple-walled ZnO piezoelectric Timoshenko beam on elastic Pasternak foundation is analytically investigated under magneto-electro-thermo-mechanical loadings. Using the Timoshenko beam free body diagram, the equilibrium equation of Timoshenko nano-beam model is obtained and solved by Navier's method for a simply-supported nano-beam. The surrounding elastic mediums are simulated by Winkler and Pasternak models and interlayer forces are considered by Lenard-Jones potential. The effects of various parameters including the elastic medium, small scale, length, thickness, van der Waals force on the critical buckling load and non-dimensional natural frequency of triple-walled ZnO nano-beam are investigated. The results of this study show that the critical buckling load reduces with increasing the temperature change, direct electric field, magnetic field, and length of nanotube, and vice versa for the thickness of nanotubes, and two parameters elastic foundations. Also, the non-local critical buckling load and non-dimensional natural frequency of Timoshenko nano-beam are smaller than the local critical buckling load and non-dimensional natural frequency. The results can be useful for designing the smart nano-beam for MEMS and NEMS.

© 2015 Published by Semnan University Press. All rights reserved.

1. Introduction

The piezoelectric thin films have been widely used in transducers, actuators, and resonators. The piezoelectric transducers generate electrical signals in response to the mechanical vibrations and produce mechanical energy in response to the electrical signals. In addition, the piezoelectric thin films have been used in sensors, Micro-Electro-Mechanical Systems (MEMSs), and Nano-Electro-Mechanical Systems (NEMSs). The piezoelectric ZnO layer has large electromechanical coupling coefficients; furthermore, it can be epitaxial growth on the high acoustic velocity substrates at a relatively low temperature, which makes it a promising candidate for the multi-layers thin film acoustic devices. Nano science is developing rapidly and this development is due to

the interest of many researchers in the various structures, such as nano-beam, graphene sheet, and nano-shell that the small scale effect plays an important role at nano scale.

The non-local elasticity theory was presented first by Eringen [1] in 1983. So many researches in the field of Piezoelectricity analysis are done by researchers [2]. The wave propagation in Single-Walled Carbon NanoTube (SWCNT) is investigated by Narendar et al. [3] under the longitudinal magnetic field using nonlocal Euler-Bernoulli beam theory. They investigated the effect of longitudinal magnetic field on wave dispersion characteristics of an equivalent continuum structure of the SWCNT embedded in an elastic medium. Their obtained results show that the velocity of flexural waves in the SWCNTs increases with an increasing in the longi-

*Corresponding author, Tel.: +98-33-654119; Fax: +98-33-654119

E-mail address: mmohammadimehr@kashanu.ac.ir

tudinal magnetic field exerted on it in the frequency ranges such as 0–20 THz.

Kiani [4] studied magneto-thermo-elastic fields caused by an unsteady longitudinal magnetic field in a conducting nanowire accounting for eddy-current loss. His results reveal that the eddy-current loss plays a crucial role in dynamic elastic fields within the nanowire, particularly for low initial duration of the applied magnetic field as well as low levels of the insulation of the nanowire's surface. Ghorbanpour Arani et al. [5] investigated electro-thermo-torsional buckling of an embedded armchair Double-Walled Boron Nitride NanoTube (DWBNT) using nonlocal shear deformation shell model. Their numerical results depict that the critical buckling load decreases with considering the piezoelectric effect. In the other work, they [6] illustrated the effect of Carbon Nano-Tube (CNT) volume fraction on the magneto-thermo-electro-mechanical behavior of smart nano-composite cylinder. Their results show that increasing the CNT volume fraction enhances the strength of the nano-composite cylinder. Thermo-magneto-dynamic stresses and perturbation of magnetic field vector in a non-homogeneous hollow cylinder are presented by Kong et al. [7]. Their numerical results described the effects of the non-homogeneous exponent of material for the hollow cylinders on the response amplitude and the phase of thermo-magneto-stresses and magnetic field vector perturbation.

Murmu et al. [8] presented the axial vibration of the embedded nanorods under transverse magnetic field effects via nonlocal elastic continuum theory. They investigated the effects of an external transverse magnetic field on the axial vibration of a nanorod such as a carbon nanotube with and without the elastic medium. Wang and Li [9] investigated the nonlinear primary resonance of a nano beam with an axial initial load using the nonlocal continuum theory. They show that the resonant amplitude decreases with increasing Winkler foundation modulus and decreasing the ratio of the length to the diameter. Mohammadimehr and Rahmati [10] considered the electro-thermo-mechanical nonlocal axial vibration analysis of Single-Walled Boron-Nitride Nano Rods (SWBNRs) under the electric excitation. They obtained the constitutive equation for the nano rods under electro-thermo-mechanical loadings, then they discussed about the effects of the aspect ratio, small scale parameter, clamped-clamped and clamped-free boundary conditions on the natural frequency.

A piezoelectric ZnO-CNT nanotube under the axial strain and electrical voltage is illustrated by Zhang et al. [11]. Their numerical results show that the critical buckling axial decreases as the length of ZnO-CNT and the applied voltage increase Akbari

Alashti et al. [12] studied the thermo-elastic analysis of a functionally graded spherical shell with the piezoelectric layers Using Differential Quadrature Method (DQM). They obtained the effects of the power index of material properties; temperature change and thickness of piezoelectric layers on stress and displacement were presented. Nonlinear softening and hardening nonlocal bending stiffness of an initially curved monolayer graphene sheet are illustrated by Jomehzadeh et al. [13]. They find out that the bending stiffness of graphene strongly depends on the initial configuration, showing no obvious maxima and minima, and suggesting the possibility of a smart tuning.

Lei et al. [14] presented the asymptotic frequencies of various damped nonlocal beams and plates. They investigated the asymptotic frequencies of four kinds of nonlocal viscoelastic damped structures, including an Euler–Bernoulli beam with rotary inertia, a Timoshenko beam, a Kirchhoff plate with rotary inertia and a Mindlin plate. Mohammadimehr et al. [15] investigated biaxial buckling and bending of smart nanocomposite plate reinforced by carbon nanotube under electro-magneto-mechanical loadings based on the extended mixture rule approach. Their results indicate that the nonlocal deflection of the smart nanocomposite plate decreases with an increase in the magnetic field intensity. Ansari et al. [16] studied the free vibration of size-dependent functionally graded microbeams based on using the strain gradient Reddy beam theory. They observe that the critical buckling loads and natural frequencies predicted by the beam models based on the MSGT and CT are the maximum and minimum values, respectively. Also, it is shown that increasing the material property gradient index leads to lower non-dimensional natural frequencies.

Najar et al. [17] developed the nonlinear nonlocal analysis of the electrostatic nanoactuators. Their simulated results show that the effect of the initial deflection seems to be reproducing frequency veering. Reddy and El-Borgi [18] obtained the Eringen's nonlocal theories of beams accounting for moderate rotations. Their numerical results for bending response are presented to illustrate the parametric effect of boundary conditions and the influence of the nonlocal parameter. It is shown that for all beams, except for those beams for which both the transverse displacement and slope are not specified at a boundary point, the nonlocal parameter has the effect of increasing the deflections.

Adhikari et al. [19] reported the nonlocal normal modes in the nanoscale dynamical systems. Their theoretical results are applied to three representative problems, namely (a) an axial vibration of a single-walled carbon nanotube, (b) a bending vibration of a double-walled carbon nanotube, and (c) a

transverse vibration of a single-layer graphene sheet. The DQM for a nonlinear nonlocal buckling analysis of a Double Layer Graphene Sheet (DLGS) integrated with the ZnO piezoelectric layers are studied by Ghorbanpour Arani et al. [20]. Their results present that the intensifying magnetic field makes the system more stable. Furthermore, increasing the thickness of both piezoelectric and graphene layers makes the system stiffer, and consequently the critical buckling load becomes more. The thermal postbuckling behavior of the size-dependent Functionally Graded (FG) Timoshenko microbeams is studied by Ansari et al. [21]. They illustrated influences of the material gradient index, length scale parameter, and boundary conditions on the thermal postbuckling behavior of FG microbeams are comprehensively investigated and also, considered the effect of geometrical imperfection on the buckling deformation of microbeams in prebuckled and postbuckled states.

Karlicic et al. [22] analyzed the dynamics of multiple viscoelastic carbon nanotube based on nanocomposites with an axial magnetic field. Their results show that the influence of the longitudinal magnetic field on the free vibration response of viscoelastically coupled multi-nanobeam system (MNBS) and discussed in details. An enhanced performance of a ZnO nanowire-based self-powered glucose sensor by piezotronic effect is reported by Yu et al. [23]. Their results show that the performance of the glucose sensor is generally enhanced by the piezotronic effect when applying a -0.79% compressive strain on the device, and magnitude of the output signal is increased by more than 200%; the sensing resolution and sensitivity of sensors are improved by more than 200% and 300%, respectively. Liew et al. [24] presented the postbuckling of the carbon nanotube-reinforced functionally graded cylindrical panels under axial compression using a meshless approach. They used several numerical cases to study the effect of various parameters including the carbon nanotube volume fraction, length-to-thickness ratio and radius on the postbuckling behaviour of CNTR-FG cylindrical panels.

Mohammadimehr et al. [25] investigated the free vibration of viscoelastic double-bonded polymeric nanocomposite plates reinforced by Functionally Graded Carbon Nanotube reinforced composites (FG-SWCNTs) using a Modified Strain Gradient Theory (MSGT), sinusoidal shear deformation theory and meshless method. Their results show that the elastic foundation, van der Waals (vdW) interaction and magnetic field increase the dimensionless natural frequency of the double-bonded nanocomposite plates for Classical Theory (CT), Modified Couple Stress Theory (MCST) and MSGT. Also, the material length scale parameter effects on the non-

dimensional natural frequency of the double bonded nano-composite plates are negligible at $h/l \geq 5$ for CT, and MCST and MSGT. In the other study, Mohammadimehr et al. [26] investigated the size dependent effect on the buckling and vibration analysis of double-bonded nanocomposite piezoelectric plate reinforced by Boron Nitride Nano-Tube (BNNT) based on MCST. The results of their research show that the critical buckling load decreases with an increase in the dimensionless material length scale parameter.

The vibration of nonlinear graduation of nano-Timoshenko beam considering the neutral axis position is studied by Eltaher et al. [27]. Their obtained numerical results reflected the significant effect of neutral axis position, material distribution profile, and the nonlocality parameter on the fundamental frequencies of the nano-Timoshenko beams. The exact buckling solution for the two-layer Timoshenko beams with interlayer slip is presented by Le Grogneq et al. [28]. It is shown that their results are in much better agreement with the numerical values than the obtained solutions with the simplified kinematic assumptions. Aydogdu [29] analyzed the propagation of longitudinal waves in the multi-walled carbon nanotubes using non-local theory. He studied the effects of van der Waals force, scale parameter and radius on the wave propagation. Ghorbanpour Arani et al. [30] studied visco-surface-nonlocal piezoelectricity effects on the nonlinear dynamic stability of the graphene sheets integrated with ZnO sensors and actuators using a refined zig-zag theory. The results depict that the magnetic field and external voltage are effective controlling parameters for dynamic instability region of system.

Ghannadpour et al. [31] examined the stress analysis, buckling and vibrations of Euler-Bernoulli beam. They developed analytical formulas to find buckling stiffness matrix and mass matrix, and then, they obtained the critical buckling load, natural frequency and deflection using Ritz method and desired boundary conditions. Wang and Adhikari [32] studied vibration analysis of the composite nanotubes synthesized by coating CNTs with piezoelectric ZnO. Their results show that the half wave number related to deformation energy, does not have observable influence on the vibration. Also the vdW interaction can play a predominant role in the mechanics of the nanostructures. Rahmati and Mohammadimehr [33] investigated the vibration analysis of the non-uniform and non-homogeneous Boron Nitride Nano-Rod (BNNR) embedded in an elastic medium under combined loadings using DQM. They conclude that the non-dimensional frequency ratio of nonhomogeneous BNNR decreases with the presence of electro-thermal loadings, and their ef-

fect on the nondimensional frequency ratio is higher in short nanorods and high nonlocal parameter.

In this study, the nonlocal buckling and vibration analysis of triple-walled ZnO piezoelectric Timoshenko nano-beam is subjected to magneto-electro-thermo-mechanical loadings. The equilibrium equation using Timoshenko beam free body diagram and writing equilibrium equation of force and momentum are achieved and solved by Navier's method for a simply-supported nano-beam. Also, the effects of various factors including the elastic medium, small scale, length, thickness, interlayer van der Waals force on the critical buckling load and natural frequency of triple-walled ZnO nanotube are investigated.

2. Triple-Walled Timoshenko Beam Model

In this article, the triple-walled ZnO piezoelectric nano-beam model is investigated based on the Timoshenko nano-beam theory. As an improvement of the multi-Euler beam model, the multi-Timoshenko beam model is proposed. In this model, each nanotube is simulated by a Timoshenko beam that allows for the effects of transverse shear deformation and rotary inertia. The deflections of the adjacent tubes are coupled through the van der Waals force and elastic foundation which are determined by the interlayer spacing. A schematic configuration of the ZnO piezoelectric Timoshenko nano-beam has been illustrated in Fig. 1.

The displacement fields for the Timoshenko beam model can be considered as follows [34]:

$$\begin{aligned} U(x, z, t) &= z\varphi(x, t) \\ V(x, z, t) &= 0 \\ W(x, z, t) &= w(x, t) \end{aligned} \quad (1)$$

where w is displacement component at the mid-surface of the beam, φ is the section normal vector rotations about the y -, and t denotes time.

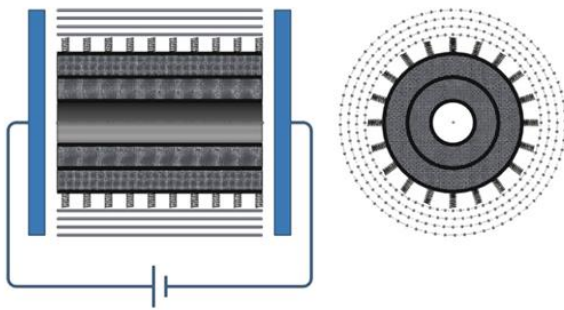


Figure 1. A schematic configuration of the ZnO piezoelectric Timoshenko nano-beam

Consider the element of the Timoshenko beam shown in Figure 2. The angle γ denotes the shear deformation of the element so we have what follows, from Figure 2 [35].

$$\gamma = \left(\varphi - \frac{\partial w}{\partial x} \right) \quad (2)$$

The bending moment M and the shear force V are written as follows:

$$\begin{aligned} M &= EI \frac{\partial \varphi}{\partial x} \\ V &= kAG\gamma = kAG\left(\varphi - \frac{\partial w}{\partial x}\right) \end{aligned} \quad (3)$$

Where w and φ are the transverse displacement, the slope of the beam due to bending deformation alone, respectively, x , I , A , E , G , and k denote the axial coordinate, the area moment of inertia, the cross-sectional area, the Young's modulus, the shear modulus and the shear correction factor (which are dependent on the shape of the cross section), respectively. Since the triple-walled ZnO piezoelectric Timoshenko nano-beam is modelled as a single beam with hollow annular cross section area, the dependence of the shear correction factor k on its cross-sectional shape is considered, and is determined by the following formula [36]:

$$k = \frac{6(1+\nu)(1+\eta)^2}{(7+6\nu)(1+\eta)^2 + (20+12\nu)\eta^2} \quad (4-a)$$

where $\eta = \frac{2R-t}{2R+t} \approx 0$ is the ratio of the innermost and

the outermost diameters of the tube; therefore, k equals what follows:

$$k = \frac{6(1+\nu)}{(7+6\nu)} \quad (4-b)$$

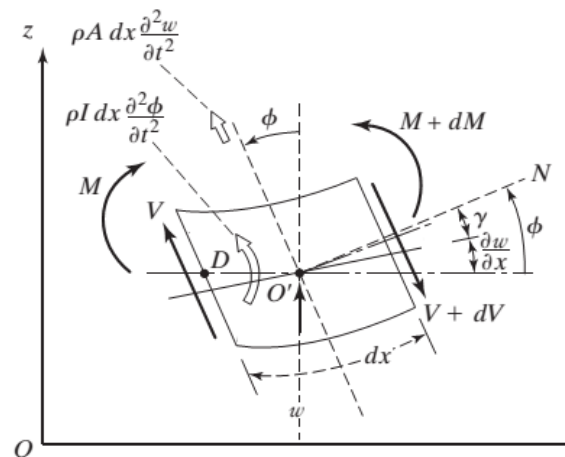


Figure 2. A schematic view of the Timoshenko beam element [35]

2.1. Governing equation of motion

Based on the Eringen's elasticity theory, the non-local constitutive formulation can be expressed in the following form:

$$\left[1 - (e_0 a)^2 \nabla^2\right] \sigma_x^{nl} = \sigma_x' \quad (5)$$

Where σ_x^{nl} and σ_x' represent the nonlocal and local stress, respectively, ∇^2 is the Laplacian operator; e_0 and a are a constant associated with each material and the internal characteristic length, respectively.

So, the governing equations of motion for ZnO piezoelectric Timoshenko nano-beam can be obtained by equations that are mentioned in Appendix A. [35, 37]:

$$\begin{aligned} & EI \frac{\partial^4 w}{\partial x^4} + \left[1 - (e_0 a)^2 \frac{\partial^2}{\partial x^2}\right] \left[1 - \frac{EI}{kAG} \frac{\partial^2}{\partial x^2}\right] q(x) + \\ & \left[1 - (e_0 a)^2 \frac{\partial^2}{\partial x^2}\right] P \frac{\partial^2 w}{\partial x^2} + \rho A \left[1 - (e_0 a)^2 \frac{\partial^2}{\partial x^2}\right] \frac{\partial^2 w}{\partial x^2} - \\ & \rho I \left[1 + \frac{E}{kG}\right] \left[1 - (e_0 a)^2 \frac{\partial^2}{\partial x^2}\right] \frac{\partial^4 w}{\partial x^2 \partial t^2} + \\ & \frac{\rho I}{KAG} \left[1 - (e_0 a)^2 \frac{\partial^2}{\partial x^2}\right] \left[1 - (e_0 a)^2 \frac{\partial^2}{\partial x^2}\right] \frac{\partial^2 q(x)}{\partial t^2} + \\ & \frac{\rho^2 I}{KG} \left[1 - (e_0 a)^2 \frac{\partial^2}{\partial x^2}\right] \left[1 - (e_0 a)^2 \frac{\partial^2}{\partial x^2}\right] \frac{\partial^4 w}{\partial t^4} = 0 \end{aligned} \quad (6)$$

Finally, for the triple-walled ZnO piezoelectric Timoshenko nano-beam, the governing equations of motion are written as follows using Eq. (6):

$$\begin{cases} EI_1 \frac{\partial^4 w_1}{\partial x^4} + \left[1 - (e_0 a)^2 \frac{\partial^2}{\partial x^2}\right] \left[1 - \frac{EI_1}{kA_1 G} \frac{\partial^2}{\partial x^2}\right] q_1(x) + \left[1 - (e_0 a)^2 \frac{\partial^2}{\partial x^2}\right] P_1 \frac{\partial^2 w_1}{\partial x^2} + \\ \rho A_1 \left[1 - (e_0 a)^2 \frac{\partial^2}{\partial x^2}\right] \frac{\partial^2 w_1}{\partial x^2} - \rho I_1 \left[1 + \frac{E}{kG}\right] \left[1 - (e_0 a)^2 \frac{\partial^2}{\partial x^2}\right] \frac{\partial^4 w_1}{\partial x^2 \partial t^2} + \\ \frac{\rho I_1}{KA_1 G} \left[1 - (e_0 a)^2 \frac{\partial^2}{\partial x^2}\right] \left[1 - (e_0 a)^2 \frac{\partial^2}{\partial x^2}\right] \frac{\partial^2 q_1(x)}{\partial t^2} + \\ \frac{\rho^2 I_1}{KG} \left[1 - (e_0 a)^2 \frac{\partial^2}{\partial x^2}\right] \left[1 - (e_0 a)^2 \frac{\partial^2}{\partial x^2}\right] \frac{\partial^4 w_1}{\partial t^4} = 0 \end{cases} \quad (7-a)$$

$$\begin{cases} EI_2 \frac{\partial^4 w_2}{\partial x^4} + \left[1 - (e_0 a)^2 \frac{\partial^2}{\partial x^2}\right] \left[1 - \frac{EI_2}{kA_2 G} \frac{\partial^2}{\partial x^2}\right] q_2(x) + \left[1 - (e_0 a)^2 \frac{\partial^2}{\partial x^2}\right] P_2 \frac{\partial^2 w_2}{\partial x^2} + \\ \rho A_2 \left[1 - (e_0 a)^2 \frac{\partial^2}{\partial x^2}\right] \frac{\partial^2 w_2}{\partial x^2} - \rho I_2 \left[1 + \frac{E}{kG}\right] \left[1 - (e_0 a)^2 \frac{\partial^2}{\partial x^2}\right] \frac{\partial^4 w_2}{\partial x^2 \partial t^2} + \\ \frac{\rho I_2}{KA_2 G} \left[1 - (e_0 a)^2 \frac{\partial^2}{\partial x^2}\right] \left[1 - (e_0 a)^2 \frac{\partial^2}{\partial x^2}\right] \frac{\partial^2 q_2(x)}{\partial t^2} + \\ \frac{\rho^2 I_2}{KG} \left[1 - (e_0 a)^2 \frac{\partial^2}{\partial x^2}\right] \left[1 - (e_0 a)^2 \frac{\partial^2}{\partial x^2}\right] \frac{\partial^4 w_2}{\partial t^4} = 0 \end{cases} \quad (7-b)$$

$$\begin{cases} EI_3 \frac{\partial^4 w_3}{\partial x^4} + \left[1 - (e_0 a)^2 \frac{\partial^2}{\partial x^2}\right] \left[1 - \frac{EI_3}{kA_3 G} \frac{\partial^2}{\partial x^2}\right] q_3(x) + \left[1 - (e_0 a)^2 \frac{\partial^2}{\partial x^2}\right] P_3 \frac{\partial^2 w_3}{\partial x^2} + \\ \rho A_3 \left[1 - (e_0 a)^2 \frac{\partial^2}{\partial x^2}\right] \frac{\partial^2 w_3}{\partial x^2} - \rho I_3 \left[1 + \frac{E}{kG}\right] \left[1 - (e_0 a)^2 \frac{\partial^2}{\partial x^2}\right] \frac{\partial^4 w_3}{\partial x^2 \partial t^2} + \\ \frac{\rho I_3}{KA_3 G} \left[1 - (e_0 a)^2 \frac{\partial^2}{\partial x^2}\right] \left[1 - (e_0 a)^2 \frac{\partial^2}{\partial x^2}\right] \frac{\partial^2 q_3(x)}{\partial t^2} + \\ \frac{\rho^2 I_3}{KG} \left[1 - (e_0 a)^2 \frac{\partial^2}{\partial x^2}\right] \left[1 - (e_0 a)^2 \frac{\partial^2}{\partial x^2}\right] \frac{\partial^4 w_3}{\partial t^4} = 0 \end{cases} \quad (7-c)$$

Where p and $q(x)$ are axial and distributed transverse loads, respectively that are obtained by the following form.

$$q(x) = q^V + q^{w-p} + f \quad (7-d)$$

$$P = P^E + P^T + P^M$$

2.2. External force

The external forces can be divided into the following parts:

- Winkler and Pasternak foundations.
- One dimensional magnetic field applied to the nano-beam.
- Van der Waals interaction forces.

2.2.1. Elastic medium

The Timoshenko nano-beam is resting on an elastic foundation whose supporting action is described by Pasternak-type relationship. The Pasternak foundation force can be expressed as follows [34]:

$$q_1^{w-p} = hk_w w_1 - hk_g \frac{\partial^2 w_1}{\partial x^2} = h(k_w w_1 - k_g \frac{\partial^2 w_1}{\partial x^2}) \quad (8)$$

where w is the transverse deflection of the beam, K_w and K_g are spring and shear coefficients of the elastic foundation, respectively.

2.2.2. Magnetic field

For a nano-beam subjected to a magnetic field, H , the exerted body force can be calculated as what follows [3, 20]:

$$\begin{aligned} h &= \text{Curl}(U \times H) = \nabla \times \begin{vmatrix} u & 0 & w \\ H_x & 0 & 0 \end{vmatrix} = \\ \nabla \times (0, wH_x, 0) &= \begin{vmatrix} \frac{\partial}{\partial x} & \frac{\partial}{\partial y} & \frac{\partial}{\partial z} \\ 0 & wH_x & 0 \end{vmatrix} = \\ (-\frac{\partial}{\partial z} wH_x, 0, \frac{\partial}{\partial x} wH_x) &= (0, 0, \frac{\partial}{\partial x} wH_x) \end{aligned} \quad (9)$$

For simplifying the analysis, a longitudinal magnetic field vector is considered as $H = (H_x, 0, 0)$.

The current density (J) and the Maxwell equations are given by the following equations:

$$\begin{aligned} J &= \text{Curl}(h) = \nabla \times h = \begin{vmatrix} \frac{\partial}{\partial x} & \frac{\partial}{\partial y} & \frac{\partial}{\partial z} \\ 0 & 0 & \frac{\partial}{\partial x} wH_x \end{vmatrix} = \\ (0, -\frac{\partial}{\partial x} (\frac{\partial}{\partial x} wH_x), 0) & \\ f &= \mu(J \times h) = \mu \times \begin{vmatrix} 0 & -\frac{\partial}{\partial x} (\frac{\partial}{\partial x} wH_x) & 0 \\ H_x & 0 & 0 \end{vmatrix} = \mu H_x^2 \frac{\partial}{\partial x} (\frac{\partial w}{\partial x}) \end{aligned} \quad (10)$$

where μ is the magnetic field permeability.

Therefore, the components of Lorentz forces along the x, y and z directions are as follows:

$$f_x = 0, f_y = 0, f_z = \mu H_x^2 \left(\frac{\partial^2 w}{\partial x^2} \right) \quad (11)$$

2.2.3. Van der Waals force

As shown in Figure 1, the triple-walled ZnO piezoelectric Timoshenko nano-beam can be assumed as a set of concentric nano-beam with *vdW* interaction forces between the inner and the outer layers which are equal in the magnitude and opposite in the sign. Therefore, the *vdW* interaction forces between adjacent layers can be expressed as follows [5]:

$$\begin{cases} q_1 = q_1^v = q_{12}^v + q_{13}^v \\ q_2 = q_2^v = q_{21}^v + q_{23}^v \\ q_3 = q_3^v = q_{31}^v + q_{32}^v \end{cases} \rightarrow \begin{cases} q_{12}^v = hC^*(w_1 - w_2) \\ q_{13}^v = hC^*(w_1 - w_3) \\ q_{23}^v = hC^*(w_2 - w_3) \end{cases}$$

and

$$\begin{cases} q_{12}^v R_1 = -q_{21}^v R_2 \\ q_{13}^v R_1 = -q_{31}^v R_3 \\ q_{23}^v R_2 = -q_{32}^v R_3 \end{cases} \quad (12)$$

where C^* is *vdW* interaction coefficient. So, the forces between adjacent layers can be expressed as what follows:

$$\begin{cases} q_1 = q_{12}^v + q_{13}^v + h(k_w w_1 - k_g \frac{\partial^2 w_1}{\partial x^2}) + \mu H_x^2 \frac{\partial^2 w_1}{\partial x^2} \\ q_2 = -\frac{R_1}{R_2} q_{12}^v + q_{23}^v \\ q_3 = -\frac{R_1}{R_3} q_{13}^v - \frac{R_2}{R_3} q_{23}^v \end{cases} \quad (13-a)$$

Substituting Eq. (12) into Eq. (13-a) yields to the following equations:

$$\begin{cases} q_1 = hC^*(w_1 - w_2) + hC^*(w_1 - w_3) + h(k_w w_1 - k_g \frac{\partial^2 w_1}{\partial x^2}) + \mu H_x^2 \frac{\partial^2 w_1}{\partial x^2} \\ q_2 = hC^* \left(\left(-\frac{R_1}{R_2} \right) (w_1 - w_2) + (w_2 - w_3) \right) \\ q_3 = -\frac{R_1}{R_3} hC^*(w_1 - w_3) - \frac{R_2}{R_3} hC^*(w_2 - w_3) \end{cases} \quad (13-b)$$

The triple-walled ZnO piezoelectric Timoshenko nano-beam under the electro-thermo-mechanical loading can be considered as what follows:

$$P_x = P_x^E + P_x^T + P_x^M \quad (14-a)$$

Where superscript M , T and E indicate the mechanical, thermal and electrical components of load as what follows [38]:

$$\begin{cases} P_x^E = h_{11} E_x A \\ P_x^T = EA \alpha_x T \\ P_x^M = P \end{cases} \quad (14-b)$$

Finally, substituting Eq. (14-b) into Eq. (14-a) yields to the following expressions:

$$\begin{cases} P_1 = P_{E1} + P_{T1} + P_{M1} = h_{11} E_x A_1 + EA_1 \alpha_x T + P \\ P_2 = P_{E2} + P_{T2} + P_{M2} = h_{11} E_x A_2 + EA_2 \alpha_x T + P \\ P_3 = P_{E3} + P_{T3} + P_{M3} = h_{11} E_x A_3 + EA_3 \alpha_x T + P \end{cases} \quad (14-c)$$

3. Navier's Type Approach

The developed governing differential equations of section 2 have been solved by Navier's approach for simply supported boundary conditions. The simply supported boundary condition for nano-beam is considered as follows:

$$x=0 \text{ and } x=L: w, M_x = 0$$

The following expressions of various generalized displacements have been assumed to be as what follows:

$$\begin{pmatrix} w_1 \\ w_2 \\ w_3 \end{pmatrix} = \begin{pmatrix} A \sin(\alpha x) \\ B \sin(\alpha x) \\ C \sin(\alpha x) \end{pmatrix} e^{i\omega t} \quad (15)$$

$$\text{where } \alpha = \frac{m\pi}{l}.$$

By substituting Eq. (15) into Eq. (7), three linear algebraic equations can be obtained that are shown in Appendix B. The matrix form of Eqs. (15-a)- (15-c) is derived as follows:

$$\begin{bmatrix} a_{11} & a_{12} & a_{13} \\ a_{21} & a_{22} & a_{23} \\ a_{31} & a_{32} & a_{33} \end{bmatrix} \begin{pmatrix} w_1 \\ w_2 \\ w_3 \end{pmatrix} = \begin{pmatrix} 0 \\ 0 \\ 0 \end{pmatrix} \quad (16)$$

where the a_{ij} , $i, j = 1, 2, 3$ coefficients in Eq. (16) are shown in Appendix C.

The natural frequencies and critical buckling load are obtained from the following expression:

$$\det \begin{bmatrix} a_{11} & a_{12} & a_{13} \\ a_{21} & a_{22} & a_{23} \\ a_{31} & a_{32} & a_{33} \end{bmatrix} = 0 \quad (17)$$

4. Numerical Results and Discussions

In this paper, using the non-local elasticity theory, the buckling and free vibration analysis of triple-walled ZnO piezoelectric Timoshenko nano-beam on elastic Pasternak foundation under magneto-electro-thermo-mechanical loadings using Navier's type approach is investigated. The physical, geomet-

rical and mechanical parameters of ZnO piezoelectric Timoshenko nano-beam are considered in Table 1. The physical, geometrical and mechanical parameters of the ZnO piezoelectric Timoshenko nano-beam are considered in Table 1. In Table 2, to validate this study with the obtained results by Wu and Lai, the dimensionless natural frequencies of single-walled carbon nanotube are calculated using Navier's method, and Timoshenko beam theory for various small scale effects is employed. The results of this research are compared with the obtained results by Wu and Lai [39] for the following mechanical properties:

$$E = 1000 \text{ GPa} \quad \nu = 0.19$$

$$\rho = 2300 \frac{\text{kg}}{\text{m}^3} \quad h = 0.34 \text{ nm} \quad (18)$$

From Table 2, it can be observed that the results of current study are in good agreement with the obtained results by Wu and Lai [39] for various non-local parameters.

The effect of various loadings such as all fields (magneto-electro-thermo-mechanical fields) (cases a and b), magneto-thermo-mechanical fields (case c), and electro-thermo-mechanical fields (case d) and length of triple-walled ZnO piezoelectric Timoshenko nano-beam on the critical buckling load is investigated in Table 3. It is shown that the critical buckling load for all states occurs in $m=2$. Also, the buckling load under the combined loadings (all fields) is less than the other states, and decreases with an increase in the length of nano-beam.

This study presents the buckling and vibration behaviors of simply supported triple-walled ZnO piezoelectric Timoshenko nano-beam. The effect of various loadings on the critical buckling load of the triple-walled ZnO piezoelectric Timoshenko nano-beam is investigated in Figure 3.

Table 1. The physical, geometrical and mechanical parameters of the ZnO piezoelectric Timoshenko nano-beam [3, 5]

parameter	value	parameter	value
h	0.066 nm	L	90 nm
E	5.5 TPa	ν	0.19
K	0.5	K_g	2.071273 nN / nm
K_w	0.89995035 nN/nm ³	c^*	99.1866693 nN/nm ³
α_x	1.2e-6	R_1	1.09 nm
R_2	0.68 nm	R_3	0.256 nm
$e_0 a$	0.056 nm	h_{11}	0.95 C/m
E_x	0.2 V/m	T	200 °C
μ	4πe-7 H/m	H_x	2.23e8 A/m

It can be observed that employing the thermal, electrical and magnetic fields in longitudinal direction of the triple-walled ZnO piezoelectric Timoshenko nano-beam decreases the critical buckling load. Also, it can be observed in this figure that the difference between various loadings is more obvious in $m=2$ and the critical buckling load for all states occurs in $m=2$. In addition, it can be seen from this figure that the maximum buckling load is related to the mechanical loading, and the buckling load under combined loadings (all fields) is less than the other states.

Figures 4a and 4b demonstrate the effect of Van der Waals force on the critical buckling load and non-dimensional natural frequency of the triple-walled ZnO piezoelectric Timoshenko nano-beam under combined loadings versus longitudinal wave number. This figure illustrates that, because of the presence of Van der Waals force, the system becomes stiffer. On the other hand, the system is a more stable. Also, it is significant in these results that with considering the first and third layers of Van der Waals force, the buckling load diagram nearly doubles, but the change of critical buckling load is negligible. The effect of the external electric voltage of the ZnO piezoelectric nano-beam on the critical buckling load is demonstrated in Figure 5.

Table 2. The comparison between the results of the current study and the obtained results by Wu and Lai [39]

Vibration mode=1	$\mu = (e_0 a)^2$	Present work	Ref. [39]
$\frac{D}{h} = 3, \frac{L}{D} = 10$	0	9.7297	9.7254
	2	8.9202	8.9163
	4	8.2841	8.2804

Table 3. The effect of various loadings and length of triple-walled ZnO piezoelectric Timoshenko nano-beam

	case a L=5 nm	case b L=6 nm	case c L=5 nm	case d L=5 nm
$m=1$	107.513	114.029	107.905	107.693
$m=2$	67.637	68.979	67.954	67.783
$m=3$	94.508	76.795	94.824	94.6527
$m=4$	147.821	109.883	148.137	147.966
$m=5$	220.746	158.685	221.062	220.891
$m=6$	311.557	220.746	311.873	311.702
$m=7$	419.660	295.211	419.9767	419.805

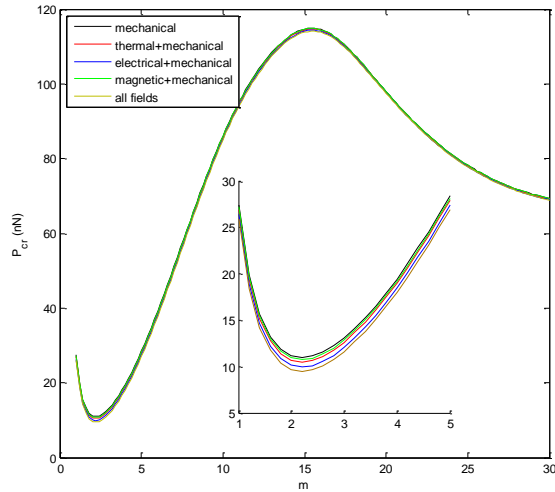
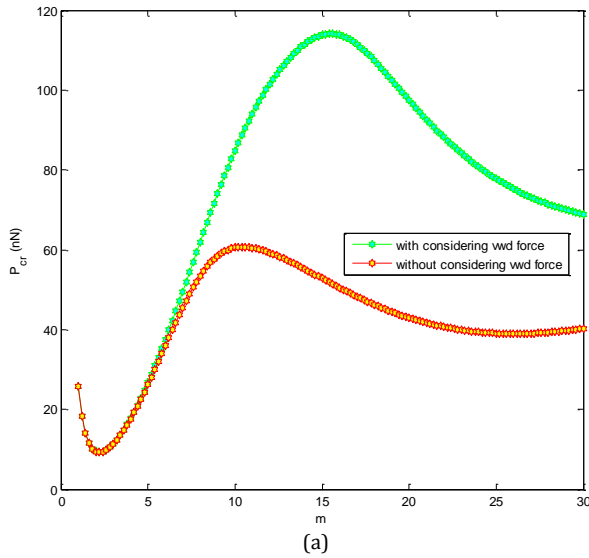
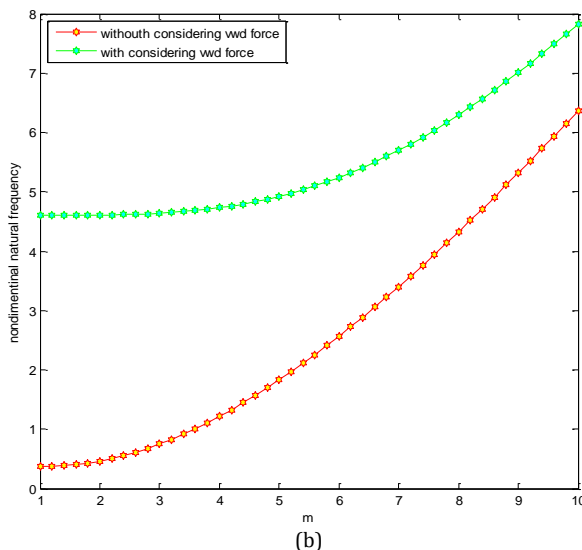


Figure 3. The effect of various loadings on the critical buckling load of the triple-walled ZnO piezoelectric Timoshenko nano-beam



(a)



(b)

Figure 4. The effect of van der Waals (vdW) force on the critical buckling load and non-dimensional natural frequency of the triple-walled ZnO piezoelectric Timoshenko nano-beam under the combined loadings versus m

It shows applying positive voltage shifts of system to lower the critical buckling load. This is due to the fact that the imposed positive and negative voltages generate the axial compressive and tensile forces in the top of ZnO piezoelectric nano-beam, respectively. Hence, the imposed external voltage is an effective controlling parameter for the dynamic stability of system.

Figure 6 shows the effect of an induced upward and downward magnetic field of the ZnO piezoelectric nano-beam on the critical buckling load. The influence of an induced upward magnetic field is more than an induced downward magnetic field. With the increasing number of longitudinal wave for $m > 10$, the difference of critical buckling load between two cases increases and it cannot be ignored, while for $m < 10$, this result is not noticeable.

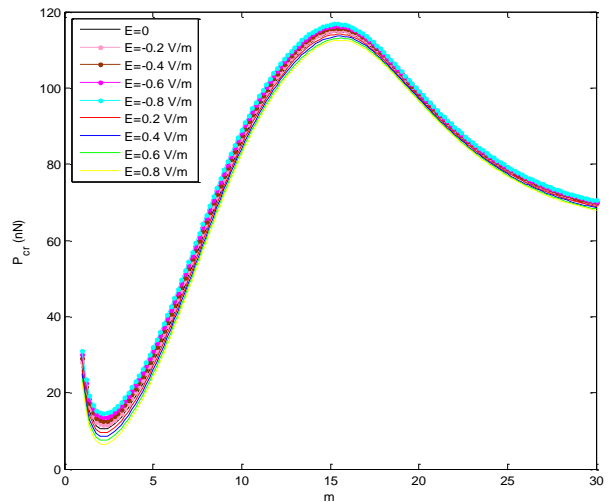


Figure 5. The effect of the external electric voltage of the ZnO piezoelectric nano-beam on the critical buckling load

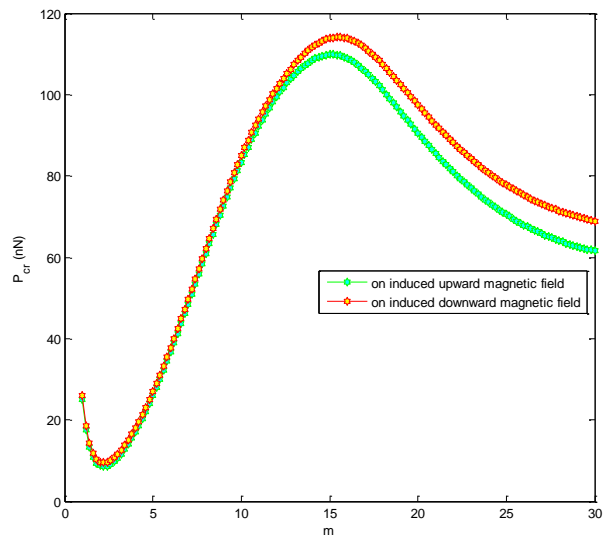


Figure 6. The effect of an induced upward and downward magnetic field of the ZnO piezoelectric nano-beam on the critical buckling load

Figs. 7a and 7b present the effect of spring constant on the critical buckling load and non-dimensional natural frequency of ZnO piezoelectric nano-beam, respectively. It is observed from the results that the critical buckling loads and the dimensionless natural frequency with increasing the spring constant increases. On the other hand, the triple-walled ZnO piezoelectric nano-beam becomes stiffer, then the stability of system enhances. Also, in this figure the slope of curves is not constant. These increases in the non-dimensional natural frequency versus the wave number are found to be almost dependent on the change of the value of the elastic layer stiffness especially at higher values. At lower values of the elastic layer stiffness, this effect is not significant.

Figs. 8a and 8b depict the local and nonlocal critical buckling and the dimensionless natural frequency loads under the magneto-electro-thermo-mechanical loading versus the axial half wave number. At nano scale, the small scale effect ($e_0 a$) is considered in formulation that this effect at macro scale is negligible, while at nano scale this parameter must be considered and this effect cannot be ignored. This effect has been shown in Figures 8a and 8b. On the other hand, in classical or local theory of continuum mechanics, the stress at a point is only proportional to the strain at that point. This theory is valid for a large scale. In a small scale, the stress at a reference point x is a function of the strain at all the other points of the body. This phenomenon is known as small-scale effect which is shown in the constitutive equations by the parameter $e_0 a$ and its theory is identified as the small-scale or non-local theory. For a structure in the nanoscale, it is not reasonable to ignore the small-scale effect ($e_0 a$). Ignoring this term ($e_0 a = 0$), the non-local theory reduces to a local or classical theory which has no desired accuracy for the analysis of CNTs. It is shown that with considering the small scale effect, the critical buckling load and non-dimensional natural frequency decrease. Moreover, the difference between the local and nonlocal critical buckling load increases with increasing the axial half wave number. It is due to the fact that the nonlocal theory introduces a more flexible model. Also, for lower values of ($e_0 a$) the critical buckling loads are higher while the critical buckling loads are lower for high-scale coefficients ($e_0 a$). It is due to the fact that the nonlocal theory introduces a more flexible model wherein the atoms are joined by the elastic springs.

Figs. 9a and 9b illustrate the effects of the length of the triple-walled ZnO piezoelectric Timoshenko nano-beam on the critical buckling load and non-dimensional natural frequency, respectively.

It is shown that with an increase in the length of the nano-beam, the instability of the system increases. Therefore, the lower length should be taken into account for ZnO in optimum design of nano/micro devices.

In Figures 10a and 10b, the effect of different values of ZnO piezoelectric nano-beam radius on the critical buckling load is investigated. According to this figure, increasing the radius of nanotubes and the number of longitudinal wave, the critical buckling load increases, and increasing the longitudinal wave number and radius, the difference between local and nonlocal theories increases.

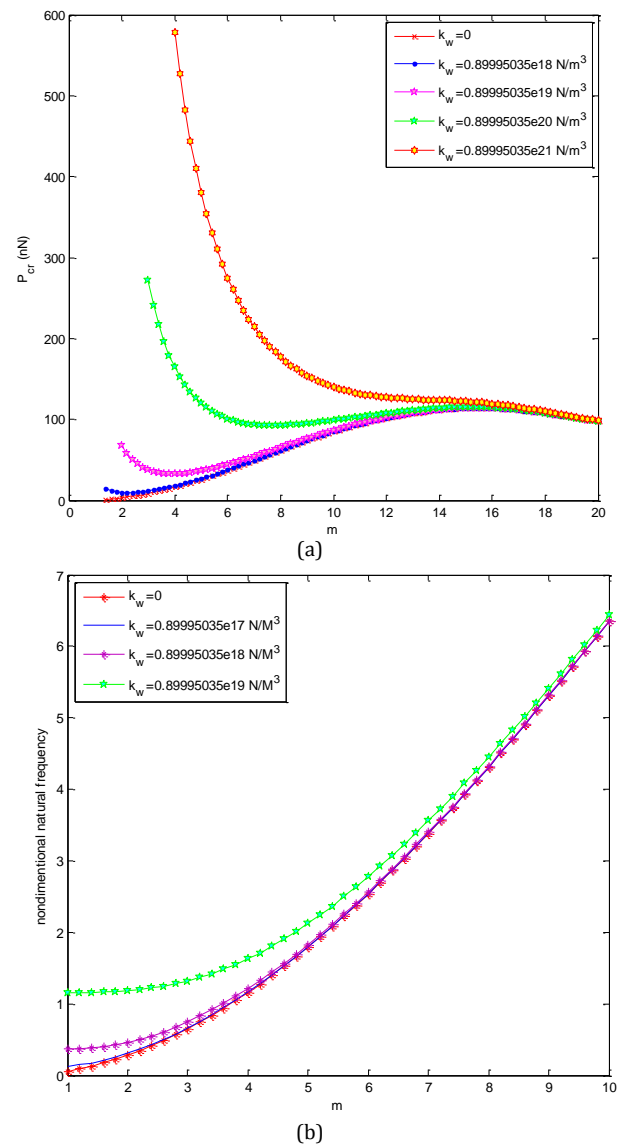


Figure 7. The effect of spring constant on the critical buckling load and non-dimensional natural frequency of the ZnO piezoelectric nano-beam

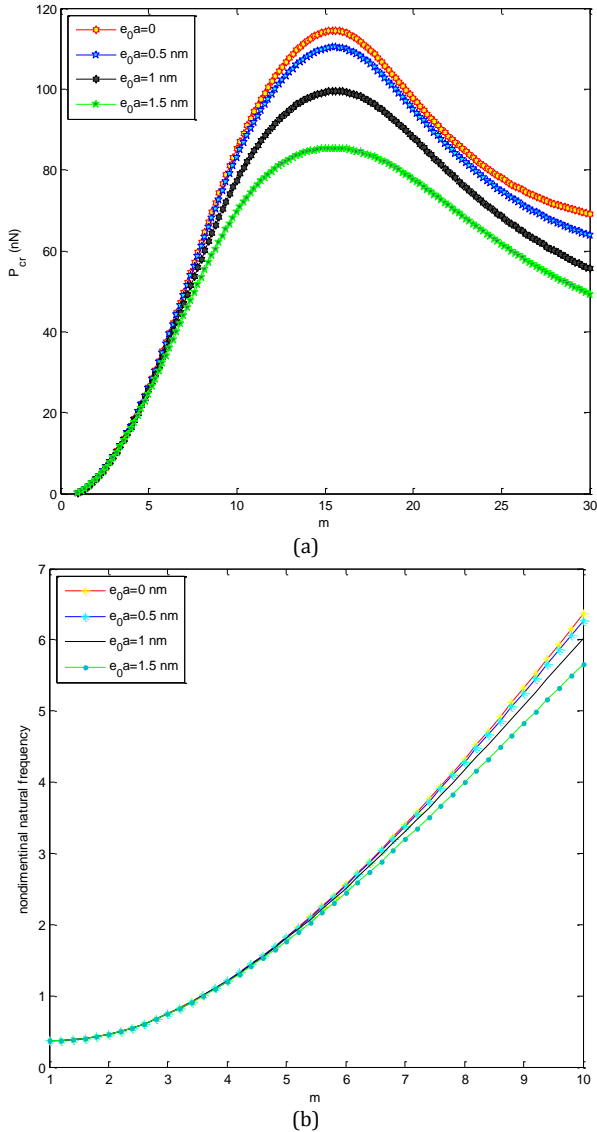


Figure 8. The effect of nonlocal parameter on the critical buckling load and non-dimensional natural frequency of the triple-walled ZnO piezoelectric nano-beam

5. Conclusion

In this study, based on the Timoshenko beam theory, the buckling and free vibration analysis of the triple-walled ZnO piezoelectric Timoshenko nano-beam on the elastic Pasternak foundation under magneto-electro-thermo-mechanical loadings is analytically investigated.

The effects of various parameters including the elastic medium, small scale parameter, length, inter-layer van der Waals force on the critical buckling load and non-dimensional natural frequency of the triple-walled ZnO piezoelectric Timoshenko nano-beam were presented.

The result of this research can be listed as follows:

1- The effects of the surrounding elastic medium, such as the spring constant of the Winkler-type and the shear constant of the Pasternak-type, as well as the vdW forces between the inner and the outer nanotubes were taken into account. Generally, the critical buckling load and non-dimensional natural frequency increase in the presence of the surrounding elastic medium, including the Winkler and Pasternak foundations. Also, the presence of van der Waals force has a positive role on the stability of the system.

2- Applying positive voltage shifts to the buckling of system to lower frequency zone and vice versa. It is also seen that the difference between various loadings is more obvious, and the critical buckling load for all states occurs in $m=2$.

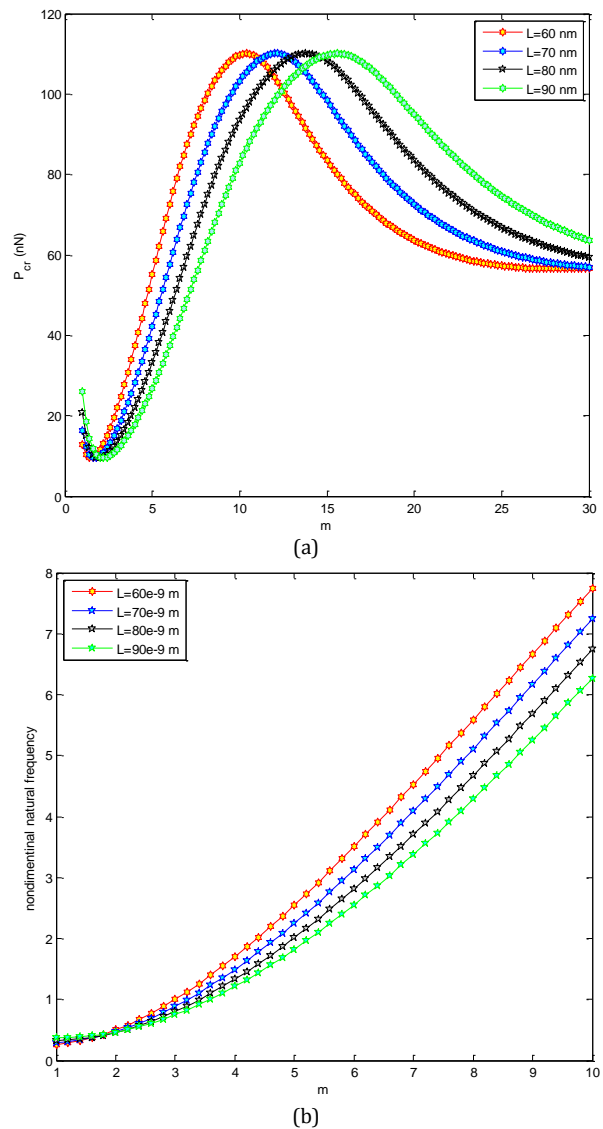


Figure 9. The effect of the length of the triple-walled ZnO piezoelectric Timoshenko nano-beam on the critical buckling load and non-dimensional natural frequency for $e_0 a = 0.5$ nm

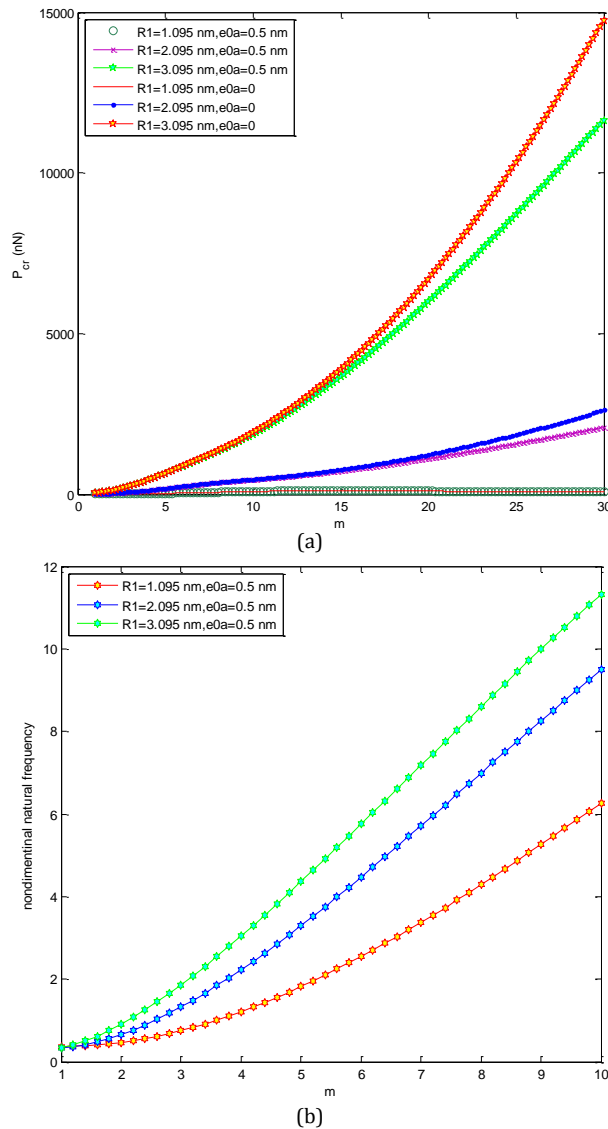


Figure 10. The effect of different values of ZnO piezoelectric nano-beam radius on the critical buckling load and non-dimensional natural frequency

3- As the system becomes stiffer, the critical buckling load becomes larger. Also it can be seen the maximum buckling load is related to the mechanical loading, and the buckling load under combined loadings (all fields) is less than the other states.

4- The influence of the small length scale on the buckling load was investigated. It is concluded that increasing the nonlocal parameter leads to a decrease in the system stability.

5- It is shown that the nonlocal critical buckling load decreases with increasing piezoelectric and magnetic field constant. On the other hand, considering the piezoelectric and magnetic fields leads to a decrease in the stability of system.

6- Increasing the radius of nanotubes and the number of longitudinal wave, the critical buckling load and dimensionless natural frequency increase.

7- With an increase in length of the beam, the instability of the system decreases.

8- The influence of an induced upward magnetic field is more than an induced downward magnetic field. It can be seen with the increasing number of longitudinal wave for $m > 10$, the difference of critical buckling load between two cases increases and it cannot be ignored, while for $m < 10$, this result is not noticeable.

9- The results of this research can be used for studying the electro thermo-mechanical buckling behavior of the smart piezoelectric nanotubes such as multi-walled BNNTs that are assumed to be surrounded by a bundle of CNTs.

Acknowledgments

The authors would like to thank the reviewers for their reports to improve the clarity of this article. Moreover, the authors are grateful to the University of Kashan for moral and financial supporting of this research by Grant No. 363452/14. They would also like to thank the Iranian Nanotechnology Development Committee for their financial support.

References

- [1] Eringen AC, on differential equations of non-local elasticity and solutions of screw dislocation and surface waves. *J Appl Phys* 1983; 54: 4703-4710.
- [2] Ying Chen, Piezoelectricity in ZnO-Based multi-layer structures for applications, New Brunswick, New Jersey May, 2008; Dissertation Director: Professor Yicheng Lu.
- [3] Narendar S, Gupta SS, Gopalakrishnan S, Wave propagation in single-walled carbon nanotube under longitudinal magnetic field using non-local Euler–Bernoulli beam theory. *Appl Math Modell* 2012; 36: 4529–4538.
- [4] Kiani K, Magneto-thermo-elastic fields caused by an unsteady longitudinal magnetic field in a conducting nanowire accounting for eddy-current loss Materials. *Chemis Phys* 2012; 136: 589–598.
- [5] Ghorbanpour Arani A, Abdollahian M, Kolahchi R, Rahmati AH, Electro-thermo-torsional buckling of an embedded armchair DWBNNT using nonlocal shear deformable shell model. *Compos Part B: Eng* 2013; 51: 291–299.
- [6] Ghorbanpour Arani A, Rahnama Mobarakeh M, Shams Sh, Mohammadimehr M, The effect of CNT volume fraction on the magneto-thermo-electro-mechanical behavior of smart nanocomposite cylinder. *J Mech Sci Tech* 2012; 26(8): 2565–2572.

- [7] Kong T, Li DX, Wanga X, Thermo-magneto-dynamic stresses and perturbation of magnetic fieldvector in a non-homogeneous hollow cylinder. *Appl Math Modell* 2009; 33: 2939–2950.
- [8] Murmu T, Adhikari S, McCarthy MA, Axial vibration of embedded nanorods under transverse magnetic field effects via nonlocal elastic continuum theory. *J Comput Theor Nanos* 2014; 11: 1–7.
- [9] Wang Yi-Ze, Li FM, Nonlinear primary resonance of nano beam with axial initial load by nonlocal continuum theory. *Int J Non-Linear Mech* 2014; 61: 74–79.
- [10] Mohammadimehr M, Rahmati AH, Small scale effect on electro-thermo-mechanical vibration analysis of single-walled boron nitride nanorods under electric excitation. *Turkis J Env Sci* 2014; 37: 1–15.
- [11] Zhang J, Wang R, Wang C, Piezoelectric ZnO-CNT nanotubes under axial strain and electrical voltage. *Physica E* 2012; 46: 105–112.
- [12] Akbari Alashti R, Khorsand M, Tarahhomi MH, Thermo-elastic analysis of a functionally graded spherical shell with piezoelectric layers by differential quadrature method. *Scientia Iranica* 2013; 20 (1):109–119.
- [13] Jomehzade E, Afshar MK, Galiotis C, Shi X, Pugno NM, Nonlinear softening and hardening nonlocal bending stiffness of an initially curved monolayer grapheme. *Int J Non-Linear Mech* 2013; 56: 123–131.
- [14] Lei Y, Adhikari S, Murmu T, Friswell MI, Asymptotic frequencies of various damped nonlocal beams and plates. *Mech Res Commun* 2014; 62: 94–101.
- [15] Mohammadimehr M, Rousta Navi B, Ghorbanpour Arani A, Biaxial buckling and bending of smart nanocomposite plate reinforced by carbon nanotube under electro-magneto-mechanical loadings based on the extended mixture rule approach. *Mech Advan Compos Struct* 2014; 1: 17–26.
- [16] Ansari R, Gholami R, Sahmani S, Free vibration of size-dependent functionally graded microbeams based on the strain gradient Reddy beam theory. *Int J Comput Meth Eng Sci Mech* 2014; 15:401–412.
- [17] Najari F, El-Borgi S, Reddy JN, Mrabet K, Nonlinear nonlocal analysis of electrostatic nanoactuators. *Compos Struct* 2015; 120:117–128.
- [18] Reddy JN, El-Borgi S, Eringen's nonlocal theories of beams accounting for moderate rotations. *Int J Eng Sci* 2014; 82: 159–177.
- [19] Adhikari S, Gilchrist D, Murmu T, McCarthy MA, Nonlocal normal modes in nanoscale dynamical systems. *Mech Syst Signal Pr* 2015; 60: 583–603.
- [20] Ghorbanpour Arani A, Fereidoon A, Kolahchi R, Nonlocal DQM for a nonlinear buckling analysis of DLGSs integrated with ZnO piezoelectric layers. *J Appl Mech* 2014; 45(1): 9-22.
- [21] Ansari R, Faghieh Shojaei M, Gholami R, Mohammadi V, Darabi MA, Thermal postbuckling behavior of size-dependent functionally graded Timoshenko microbeams. *Int J Non-Linear Mech* 2013; 50: 127–135.
- [22] Karlicic D, Murmu T, Cajic M, KozicP, Adhikari S, Dynamics of multiple viscoelastic carbon nanotube based nanocomposites with axial magnetic field. *J Appl Phys* 2014; 115: 234–303.
- [23] Yu R, Pan C, Chen J, Zhu G, Wang ZL, Enhanced Performance of a ZnO Nanowire-Based Self-Powered Glucose Sensor by Piezotronic Effect. *Advan Func Mater*, 2013; doi:10.1002/adfm.201300593/j.adv.funct.mat. 2013.
- [24] Liew KM, Lei ZX, Yu JL, Zhang LW, Postbuckling of carbon nanotube-reinforced functionally graded cylindrical panels under axial compression using a meshless approach. *Comput Methods Appl Mech Eng* 2014; 268: 1–17.
- [25] Mohammadimehr M, Rousta Navi B, Ghorbanpour Arani A, The free vibration of viscoelastic double-bonded polymeric nanocomposite plates reinforced by FG-SWCNTs using modified strain gradient theory (MSGT) sinusoidal shear deformation theory and meshless method. *Compos Struct* 2015; 131: 654–671.
- [26] Mohammadimehr M, Mohandes M, Moradi M, Size dependent effect on the buckling and vibration analysis of double-bonded nanocomposite piezoelectric plate reinforced by boron nitride nanotube based on modified couple stress theory. *J Vib Control*; doi:10.1177/1077546314544513/j.vib.cont. 2014.
- [27] Eltahir MA, Abdelrahman AA, Al-Nabawy A, Khater M, Mansour A, Vibration of nonlinear graduation of nano-Timoshenko beam considering the neutral axis position. *Appl Math Comput* 2014; 235: 512–529.
- [28] Le Grogne P, Nguyen Q, Hjjaj M, Exact buckling solution for two-layer Timoshenko beams with interlayerslip. *Int J Solids Struct*, 2012; 49: 143–150.
- [29] Aydogdu M, Longitudinal wave propagation in multi-walled carbon nanotubes. *Compos Struct* 2014; 107: 578–584.
- [30] Ghorbanpour Arani A, Kolahchi R, Zarei ShM, Visco-surface-nonlocal piezoelectricity effects on nonlinear dynamic stability of graphene sheets integrated with ZnO sensors and actua-

tors using refined zigzag theory. *Compos Struct* 2015; 132: 506–526.

- [31] Ghannadpour SAM, Mohammadi B, Fazilati J, Bending, buckling and vibration problems of nonlocal Euler beams using Ritz method. *Compos Struct* 2013; 96: 584–589.
- [32] Wang ChY, Adhikari S, ZnO-CNT composite nanotubes as nanoresonators. *Phys Lett A* 2011; 375: 2171–2175.
- [33] Rahmati AH, Mohammadimehr M, Vibration analysis of non-uniform and non-homogeneous boron nitride nanorods embedded in an elastic medium under combined loadings using DQM. *Physica B* 2014; 440: 88–98.
- [34] Yas MH, Samadi N, Free vibrations and buckling analysis of carbon nanotube-reinforced composite Timoshenko beams on elastic foundation. *Int J Pres Ves Pip* 2012; 98: 119–128.
- [35] Rao SS, **Mechanical Vibration: Theory and Analysis**, Prentice Hall, 2011.
- [36] Wang CM, Tan VBC, Zhang YY, Timoshenko beam model for vibration analysis of multi-walled carbon nanotubes. *J Sound Vib* 2012; 294:1060–1072.
- [37] Mohammadimehr M, Saidi AR, Ghorbanpour Arani A, Arefmanesh A, Han Q, Buckling analysis of double-walled carbon nanotubes embedded in an elastic medium under axial compression using non-local Timoshenko beam theory. *J Mech Eng Sci* 2011; 225: 498–506.
- [38] Ghorbanpour Arani A, Hashemian M, Kolahchi R, Time discretization effect on the nonlinear vibration of embedded SWBNNT conveying viscous fluid. *Compos: Part B* 2013; 54: 298–306.
- [39] Wu CP, Lai ww. Free vibration of an embedded single-walled carbon nanotube with various boundary conditions using the RMVT-based nonlocal Timoshenko beam theory and DQ method. *Physica E* 2015; 68: 8–21.

Appendix A

To decouple the equations of motion, the following manner should be considered.

The shear force and moment for nonlocal Timoshenko nano-beam are considered as follows [40]:

$$\left[1-(e_0a)^2 \frac{\partial^2}{\partial x^2}\right] V = kAG(\varphi - \frac{\partial w}{\partial x}) \tag{A-1}$$

$$\left[1-(e_0a)^2 \frac{\partial^2}{\partial x^2}\right] M = EI \frac{\partial \varphi}{\partial x} \tag{A-2}$$

The equations of motions are written as follows:

$$\sum F_z = ma_z \Rightarrow q(x,t) + \frac{\partial V}{\partial x} = -\rho A \frac{\partial^2 w}{\partial t^2} \tag{A-3}$$

$$\sum M_0 = I\ddot{\varphi} \Rightarrow V = \frac{\partial M}{\partial x} + \rho \frac{\partial w}{\partial x} - \rho I \frac{\partial^2 \varphi}{\partial t^2} \tag{A-4}$$

Substituting Eqs. (A-1) and (A-2) into Eqs. (A-3) and (A-4), one can obtain the following equations:

$$kAG\left(\frac{\partial \varphi}{\partial x} - \frac{\partial^2 w}{\partial x^2}\right) = EI \frac{\partial^3 \varphi}{\partial x^3} + \rho \left[1-(e_0a)^2 \frac{\partial^2}{\partial x^2}\right] \frac{\partial^2 w}{\partial x^2} - \tag{A-5}$$

$$\rho I \left[1-(e_0a)^2 \frac{\partial^2}{\partial x^2}\right] \frac{\partial^3 \varphi}{\partial x \partial t^2} - q(x,t) \left[1-(e_0a)^2 \frac{\partial^2}{\partial x^2}\right] - \rho A \left[1-(e_0a)^2 \frac{\partial^2}{\partial x^2}\right] \frac{\partial^2 w}{\partial t^2} = EI \frac{\partial^3 \varphi}{\partial x^3} + \rho \left[1-(e_0a)^2 \frac{\partial^2}{\partial x^2}\right] \frac{\partial^2 w}{\partial x^2} - \rho I \left[1-(e_0a)^2 \frac{\partial^2}{\partial x^2}\right] \frac{\partial^3 \varphi}{\partial x \partial t^2} \tag{A-6}$$

Differentiating Eq. (A-1) with respect to the independent variable x three times, we have:

$$\frac{\partial^3 \varphi}{\partial x^3} = \frac{\left[1-(e_0a)^2 \frac{d^2}{dx^2}\right] \frac{\partial^3 V}{\partial x^3}}{kAG} + \frac{\partial^4 w}{\partial x^4} \tag{A-7}$$

Substituting Eq. (A-3) into Eq. (A-7), the following equation is derived:

$$\frac{\partial^3 \varphi}{\partial x^3} = \frac{\left[1-(e_0a)^2 \frac{\partial^2}{\partial x^2}\right] \left(-\frac{\partial^2 q}{\partial x^2} - \rho A \frac{\partial^4 w}{\partial x^2 \partial t^2}\right) + \frac{\partial^4 w}{\partial x^4}}{kAG} \tag{A-8}$$

Also, using Eqs. (A-1) and (A-3), we have:

$$\frac{\partial^3 \varphi}{\partial x \partial t^2} = \frac{\left[1-(e_0a)^2 \frac{\partial^2}{\partial x^2}\right] \left(-\frac{\partial^2 q}{\partial t^2} - \rho A \frac{\partial^4 w}{\partial t^4}\right) + \frac{\partial^4 w}{\partial x^2 \partial t^2}}{kAG} \tag{A-9}$$

Substituting Eqs. (A-8) and (A-9) into Eq. (A-6) yields the governing equation of motion for ZnO piezoelectric Timoshenko nano-beam that is shown in Eq. (6).

Appendix B

Substituting Eq. (15) into Eq. (7), three linear algebraic equations for triple-walled ZnO piezoelectric Timoshenko nano-beam can be obtained that are shown in the following form:

$$\begin{cases} EI_1 \left(\frac{m\pi}{l}\right)^4 w_1 + \left[1+(e_0a)^2 \left(\frac{m\pi}{l}\right)^2\right] \left[1 + \frac{EI_1}{kAG} \left(\frac{m\pi}{l}\right)^2\right] \\ [hC'(w_1-w_2) + C'(w_1-w_3) + k_w w_1 + \left(\frac{m\pi}{l}\right)^2 k_y w_1 - \left(\frac{m\pi}{l}\right)^2 \mu H^2 w_1] \\ - \left[1+(e_0a)^2 \left(\frac{m\pi}{l}\right)^2\right] (h_1 E_x A_1 + EA_1 \alpha_x T + P) \left(\frac{m\pi}{l}\right)^2 w_1 - \rho A_1 \omega^2 \left[1+(e_0a)^2 \left(\frac{m\pi}{l}\right)^2\right] w_1 \\ - \rho I_1 \omega^2 \left(\frac{m\pi}{l}\right)^2 \left[1 + \frac{E}{kG}\right] \left[1+(e_0a)^2 \left(\frac{m\pi}{l}\right)^2\right] w_1 - \frac{\rho I_1}{kAG} \omega^2 \left[1+(e_0a)^2 \left(\frac{m\pi}{l}\right)^2\right] \\ \left[1+(e_0a)^2 \left(\frac{m\pi}{l}\right)^2\right] [hC'(w_1-w_2) + C'(w_1-w_3) + k_w w_1 + k_y \left(\frac{m\pi}{l}\right)^2 w_1 - \left(\frac{m\pi}{l}\right)^2 \mu H^2 w_1] + \\ \frac{\rho^2 I_1}{kG} \omega^4 \left[1+(e_0a)^2 \left(\frac{m\pi}{l}\right)^2\right] \left[1+(e_0a)^2 \left(\frac{m\pi}{l}\right)^2\right] w_1 = 0 \end{cases} \tag{B-1}$$

$$\begin{cases} EI_2 \left(\frac{m\pi}{l}\right)^4 w_2 + \left[1+(e_0a)^2 \left(\frac{m\pi}{l}\right)^2\right] \times \left[1 + \frac{EI_2}{kAG} \left(\frac{m\pi}{l}\right)^2\right] \\ [hC'(-\frac{R_1}{R_2}(w_1-w_2) + (w_2-w_3)) - \left[1+(e_0a)^2 \left(\frac{m\pi}{l}\right)^2\right] (h_1 E_x A_2 + EA_2 \alpha_x T + P) \\ \left(\frac{m\pi}{l}\right)^2 w_2 - \rho A_2 \omega^2 \left[1+(e_0a)^2 \left(\frac{m\pi}{l}\right)^2\right] w_2 - \rho I_2 \omega^2 \left(\frac{m\pi}{l}\right)^2 \left[1 + \frac{E}{kG}\right] \left[1+(e_0a)^2 \left(\frac{m\pi}{l}\right)^2\right] w_2 \\ - \frac{\rho I_2}{kAG} \omega^2 \left[1+(e_0a)^2 \left(\frac{m\pi}{l}\right)^2\right] \left[1+(e_0a)^2 \left(\frac{m\pi}{l}\right)^2\right] \\ [hC'(-\frac{R_1}{R_2}(w_1-w_2) + (w_2-w_3)) + \frac{\rho^2 I_2}{kG} \omega^4 \left[1+(e_0a)^2 \left(\frac{m\pi}{l}\right)^2\right] \left[1+(e_0a)^2 \left(\frac{m\pi}{l}\right)^2\right] w_2 = 0 \end{cases} \tag{B-2}$$

$$\begin{aligned}
 & \left[EI_3 \left(\frac{m\pi}{l} \right)^4 w_3 + \left[1 + (e_o a)^2 \left(\frac{m\pi}{l} \right)^2 \right] \times \left[1 + \frac{EI_3}{kA_3 G} \left(\frac{m\pi}{l} \right)^2 \right] \right. \\
 & \left. (hC' - \frac{R_1}{R_3} (w_1 - w_3) - \frac{R_2}{R_3} (w_2 - w_3)) - \left[1 + (e_o a)^2 \left(\frac{m\pi}{l} \right)^2 \right] [h_1 E_x A_3 + EA_3 \alpha_x T + P] \right. \\
 & \left. \left(\frac{m\pi}{l} \right)^2 w_3 - \rho A_3 \omega^2 \left[1 + (e_o a)^2 \left(\frac{m\pi}{l} \right)^2 \right] w_3 - \rho I_3 \omega^2 \left(\frac{m\pi}{l} \right)^2 \left[1 + \frac{E}{kG} \right] \left[1 + (e_o a)^2 \left(\frac{m\pi}{l} \right)^2 \right] w_3 \right. \\
 & \left. - \frac{\rho I_3}{kA_3 G} \omega^2 \left[1 + (e_o a)^2 \left(\frac{m\pi}{l} \right)^2 \right] \left[1 + (e_o a)^2 \left(\frac{m\pi}{l} \right)^2 \right] \right. \\
 & \left. (hC' - \frac{R_1}{R_3} (w_1 - w_3) - \frac{R_2}{R_3} (w_2 - w_3)) + \frac{\rho^2 I_3}{kG} \omega^4 \left[1 + (e_o a)^2 \left(\frac{m\pi}{l} \right)^2 \right] \left[1 + (e_o a)^2 \left(\frac{m\pi}{l} \right)^2 \right] w_3 = 0 \right. \quad (B-3)
 \end{aligned}$$

Appendix C

The a_j , $i, j=1,2,3$ coefficients in Eq. (16) are written as follows:

$$\begin{aligned}
 & a_{11} = EI_1 \left(\frac{m\pi}{l} \right)^4 + \left[1 + (e_o a)^2 \left(\frac{m\pi}{l} \right)^2 \right] \left[1 + \frac{EI_1}{kA_1 G} \left(\frac{m\pi}{l} \right)^2 \right] \\
 & \left(h \left\{ C' + C' + k_w + k_s \left(\frac{m\pi}{l} \right)^2 \right\} - \left(\frac{m\pi}{l} \right)^2 \mu H_2^2 \right) - \left[1 + (e_o a)^2 \left(\frac{m\pi}{l} \right)^2 \right] \\
 & (h_1 E_x A_1 + EA_1 \alpha_x T + P) \left(\frac{m\pi}{l} \right)^2 - \rho A_1 \omega^2 \left[1 + (e_o a)^2 \left(\frac{m\pi}{l} \right)^2 \right] - \\
 & \rho I_1 \omega^2 \left[1 + \frac{E}{kG} \right] \left[1 + (e_o a)^2 \left(\frac{m\pi}{l} \right)^2 \right] \\
 & - \frac{\rho I_1}{kA_1 G} \omega^2 \left[1 + (e_o a)^2 \left(\frac{m\pi}{l} \right)^2 \right] \left[1 + (e_o a)^2 \left(\frac{m\pi}{l} \right)^2 \right] \\
 & \left\{ h \left\{ C' + C' + k_w + k_s \left(\frac{m\pi}{l} \right)^2 \right\} - \left(\frac{m\pi}{l} \right)^2 \mu H_2^2 \right\} + \frac{\rho^2 I_1}{kG} \omega^4 \left[1 + (e_o a)^2 \left(\frac{m\pi}{l} \right)^2 \right] \\
 & \left[1 + (e_o a)^2 \left(\frac{m\pi}{l} \right)^2 \right] \\
 & a_{12} = \left[1 + (e_o a)^2 \left(\frac{m\pi}{l} \right)^2 \right] \left[1 + \frac{EI_1}{kA_1 G} \left(\frac{m\pi}{l} \right)^2 \right] (-hC') - \frac{\rho I_1}{kA_1 G} \omega^2 \left[1 + (e_o a)^2 \left(\frac{m\pi}{l} \right)^2 \right] \\
 & \left[1 + (e_o a)^2 \left(\frac{m\pi}{l} \right)^2 \right] (-hC') \\
 & a_{13} = \left[1 + (e_o a)^2 \left(\frac{m\pi}{l} \right)^2 \right] \left[1 + \frac{EI_1}{kA_1 G} \left(\frac{m\pi}{l} \right)^2 \right] (-hC') - \frac{\rho I_1}{kA_1 G} \omega^2 \left[1 + (e_o a)^2 \left(\frac{m\pi}{l} \right)^2 \right] \\
 & \left[1 + (e_o a)^2 \left(\frac{m\pi}{l} \right)^2 \right] (-hC') \quad (C-1)
 \end{aligned}$$

$$\begin{aligned}
 & a_{21} = \left[1 + (e_o a)^2 \left(\frac{m\pi}{l} \right)^2 \right] \left[1 + \frac{EI_2}{kA_2 G} \left(\frac{m\pi}{l} \right)^2 \right] (-\frac{R_1}{R_2}) hC' - \\
 & \frac{\rho I_2}{kA_2 G} \omega^2 \left[1 + (e_o a)^2 \left(\frac{m\pi}{l} \right)^2 \right] \left[1 + (e_o a)^2 \left(\frac{m\pi}{l} \right)^2 \right] (-\frac{R_1}{R_2}) hC' \\
 & a_{22} = EI_2 \left(\frac{m\pi}{l} \right)^4 + \left[1 + (e_o a)^2 \left(\frac{m\pi}{l} \right)^2 \right] \left[1 + \frac{EI_2}{kA_2 G} \left(\frac{m\pi}{l} \right)^2 \right] \\
 & \left\{ \left(\frac{R_1}{R_2} + 1 \right) hC' \right\} - \left[1 + (e_o a)^2 \left(\frac{m\pi}{l} \right)^2 \right] [h_1 E_x A_2 + EA_2 \alpha_x T + P] \left(\frac{m\pi}{l} \right)^2 - \\
 & \rho A_2 \omega^2 \left[1 + (e_o a)^2 \left(\frac{m\pi}{l} \right)^2 \right] - \rho I_2 \omega^2 \left(\frac{m\pi}{l} \right)^2 \left[1 + \frac{E}{kG} \right] \left[1 + (e_o a)^2 \left(\frac{m\pi}{l} \right)^2 \right] - \\
 & \frac{\rho I_2}{kA_2 G} \omega^2 \left[1 + (e_o a)^2 \left(\frac{m\pi}{l} \right)^2 \right] \left[1 + (e_o a)^2 \left(\frac{m\pi}{l} \right)^2 \right] \\
 & \left\{ \left(\frac{R_1}{R_2} + 1 \right) hC' \right\} + \frac{\rho^2 I_2}{kG} \omega^4 \left[1 + (e_o a)^2 \left(\frac{m\pi}{l} \right)^2 \right] \left[1 + (e_o a)^2 \left(\frac{m\pi}{l} \right)^2 \right] \\
 & a_{23} = \left[1 + (e_o a)^2 \left(\frac{m\pi}{l} \right)^2 \right] \left[1 + \frac{EI_2}{kA_2 G} \left(\frac{m\pi}{l} \right)^2 \right] (-hC') - \frac{\rho I_2}{kA_2 G} \omega^2 \left[1 + (e_o a)^2 \left(\frac{m\pi}{l} \right)^2 \right] \\
 & \left[1 + (e_o a)^2 \left(\frac{m\pi}{l} \right)^2 \right] (-hC') \quad (C-2)
 \end{aligned}$$

$$\begin{aligned}
 & a_{31} = \left[1 + (e_o a)^2 \left(\frac{m\pi}{l} \right)^2 \right] \left[1 + \frac{EI_3}{kA_3 G} \left(\frac{m\pi}{l} \right)^2 \right] (-\frac{R_1}{R_3}) hC' - \\
 & \frac{\rho I_3}{kA_3 G} \omega^2 \left[1 + (e_o a)^2 \left(\frac{m\pi}{l} \right)^2 \right] \left[1 + (e_o a)^2 \left(\frac{m\pi}{l} \right)^2 \right] (-\frac{R_1}{R_3}) hC' \\
 & a_{32} = \left[1 + (e_o a)^2 \left(\frac{m\pi}{l} \right)^2 \right] \left[1 + \frac{EI_3}{kA_3 G} \left(\frac{m\pi}{l} \right)^2 \right] (-\frac{R_2}{R_3}) hC' - \\
 & \frac{\rho I_3}{kA_3 G} \omega^2 \left[1 + (e_o a)^2 \left(\frac{m\pi}{l} \right)^2 \right] \left[1 + (e_o a)^2 \left(\frac{m\pi}{l} \right)^2 \right] (-\frac{R_2}{R_3}) hC' \\
 & a_{33} = EI_3 \left(\frac{m\pi}{l} \right)^4 + \left[1 + (e_o a)^2 \left(\frac{m\pi}{l} \right)^2 \right] \left[1 + \frac{EI_3}{kA_3 G} \left(\frac{m\pi}{l} \right)^2 \right] \\
 & \left\{ hC' \left(\frac{R_1}{R_3} + \frac{R_2}{R_3} \right) \right\} - \left[1 + (e_o a)^2 \left(\frac{m\pi}{l} \right)^2 \right] \{ h_1 E_x A_3 + EA_3 \alpha_x T + P \} \left(\frac{m\pi}{l} \right)^2 \\
 & - \rho A_3 \omega^2 \left[1 + (e_o a)^2 \left(\frac{m\pi}{l} \right)^2 \right] - \rho I_3 \omega^2 \left(\frac{m\pi}{l} \right)^2 \left[1 + \frac{E}{kG} \right] \left[1 + (e_o a)^2 \left(\frac{m\pi}{l} \right)^2 \right] \\
 & - \frac{\rho I_3}{kA_3 G} \omega^2 \left[1 + (e_o a)^2 \left(\frac{m\pi}{l} \right)^2 \right] \left[1 + (e_o a)^2 \left(\frac{m\pi}{l} \right)^2 \right] \\
 & \left\{ hC' \left(\frac{R_1}{R_3} + \frac{R_2}{R_3} \right) \right\} + \frac{\rho^2 I_3}{kG} \omega^4 \left[1 + (e_o a)^2 \left(\frac{m\pi}{l} \right)^2 \right] \left[1 + (e_o a)^2 \left(\frac{m\pi}{l} \right)^2 \right] \\
 & \quad (C-3)
 \end{aligned}$$